Deliverable D1.4: Laser deburring cell.

Automated robotic system for laser deburring of complex 3D shape parts

Author 1 (TEKNIKER FOUNDATION)
Author 2 (IDELT S.L.)

Version 1
Submission date: 06.09.2016

1 Publishable Summary. Introduction.

The automated deburring process of parts with complex geometries usually presents many challenges. On this document the machine vision techniques, involved in the design and set up of an automated adaptive cognitive robotic system for the laser deburring of metal casting 3D high quality complex parts, and the laser deburring technology applied on the final demonstrator are explained. To carry out, autonomously, the deburring process operation, 3D machine vision techniques have been used for different purposes. These machine vision algorithms combined with industrial robots and a high tech laser cutting head, make possible the full automation of the deburring process. This setup could potentially be applied to medium sized parts of different light casting alloys.

This deliverable describes the results of the activities carried out on Task 3. Building on the previous developments of Tasks 1 and 2, the system has been set up and finely tuned in order to have the cell ready to work on real parts, integrating their actions to test that the different operations are done correctly. The integration also comprises the laser station, where the laser deburring adaptive methodology will be checked and optimized, so as to make an efficient use of the available laser power and reduce process time to its minimum.

2 Manipulation of the part. Measurement and location of burs.

2.1 Brief description of the cell.

The automatic deburring cell consists of the following components:

- Robot and grasping system
- Conveyor belt and 2D pose estimation workstation
- Burr measurement by 3D workstation
- Deburring process workstation
- Output station

All the elements are set together inside a cell within the robot working range distance. This cell operates inside an enclosure of 2.5 m height. This protects the outside from laser emissions, since the laser head works with a 200 W source, which might be dangerous for the staff working on the adjacent shop floor.

The following figures visualize the different elements of the cell. The robot is a COMAU NM-45 with a 45 Kg payload.

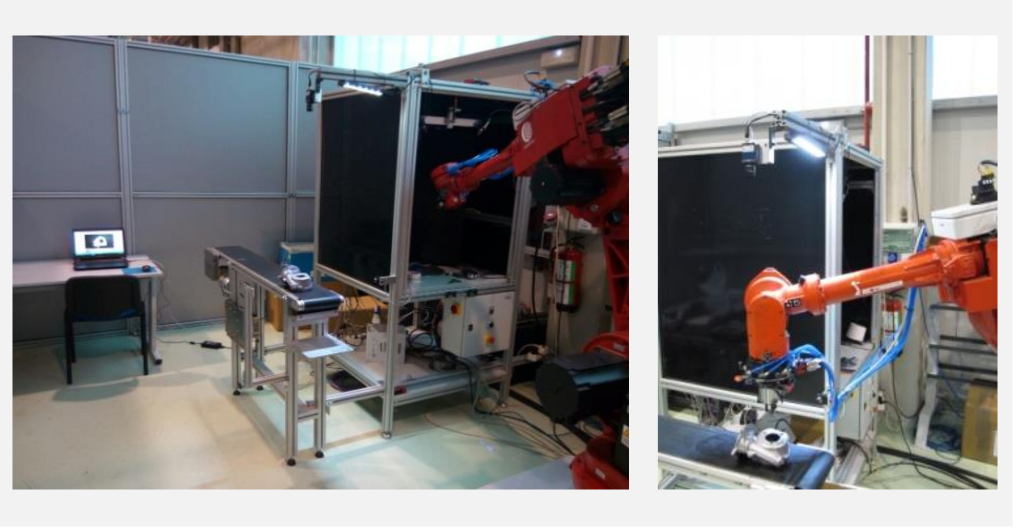

Global view of the cell. Detailed view of the vision stations.

Following DEBUR project design guidelines, the robot moves the part through the different workstations. A conveyor belt introduces the part to the cell. A photoelectric cell stops the part under a 2D camera. This is the 2D workstation, which estimates the pose of the part and passes it to the robot in order to grasp it. Once this operation is completed, the robot introduces the part inside the 3D workstation for measurement. After measurement and estimation of size and position of burrs, the part is moved to the deburring module where the laser will remove them. In the final step, the robot leaves the part in a table (parts deposition area).

2.2 Grasping: design for robot

A manual interchange system has been designed for the robot flange. This gives much more flexibility for an efficient use of the cell. It allows for the laser head to be attached to the robot for laser deburring testing or to attach the gripper for grasping testing and burr detection at 2D and 3D workstations of the cell. Three interchange systems are required: one is fixed and goes attached to the robot flange and the other two are for the removable systems, one for each case (See figures below). All needed elements, like the materials, the gripper and the interchange systems have been purchased. The mechanical interfaces, required to attach the interchange systems to the robot flange, the gripper and the laser head, have been designed and manufactured.

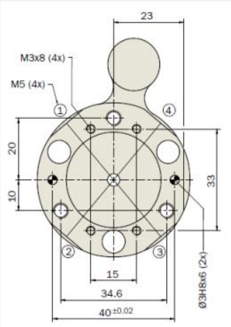

Tool fixed to the robot

Gimatic system: both sides

The selected gripper

Finally, attached to the robot flange, a grasping pneumatic gripper has been designed for the manipulation of the part. The system is valid for different parts, for that, it is enough to change the end effectors of the gripper.

Parts required for manipulation on DEBUR project have a circular ring. Due to this the gripper was designed to have three fingers. These are designed and manufactured depending on the part geometry to be grasped.

The next figures show the two parts worked out at DEBUR. In the figures, the grasping position is marked by arrows. The diameters at the grasping locations are different, so the fingers have been designed accordingly for each part.

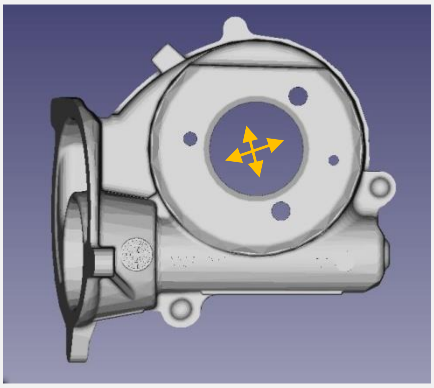

Part 1: gripping area

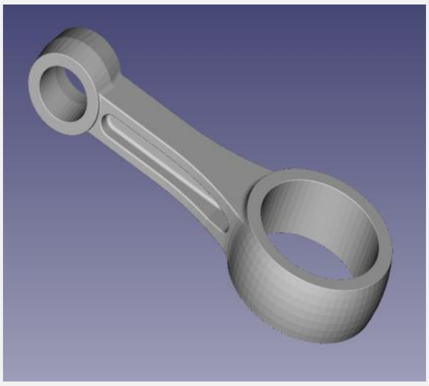

Part 2: gripping area

The final set gripper-finger is shown in the following pictures. The final gripper with the two set of fingers constructed to manipulate each part is shown.

Gripper with fingers for part 1

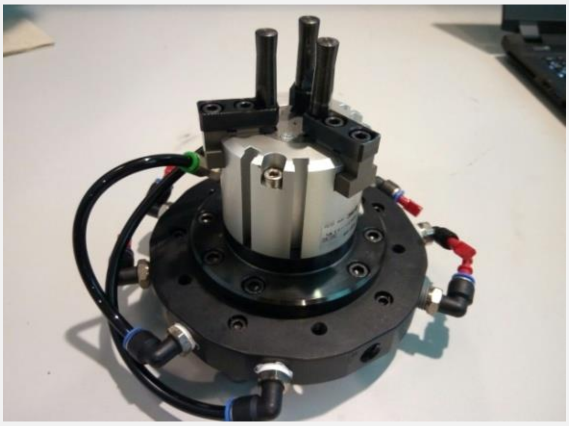

Gripper with fingers for rod

In the following pictures the grasping by the robot of the two parts is shown. Two set of fingers have been designed and constructed to allow the robot to grasp both of them using the same pneumatic grip device.

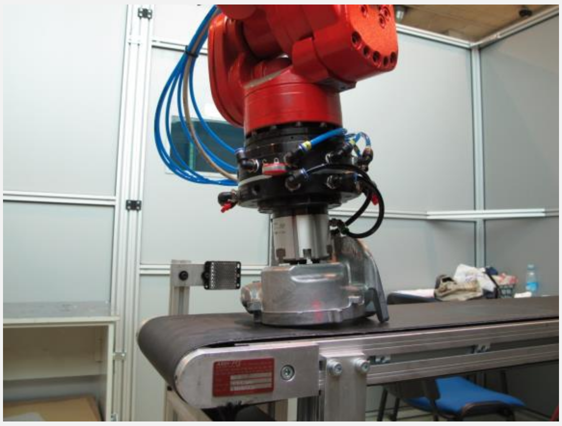

Grasping part 1

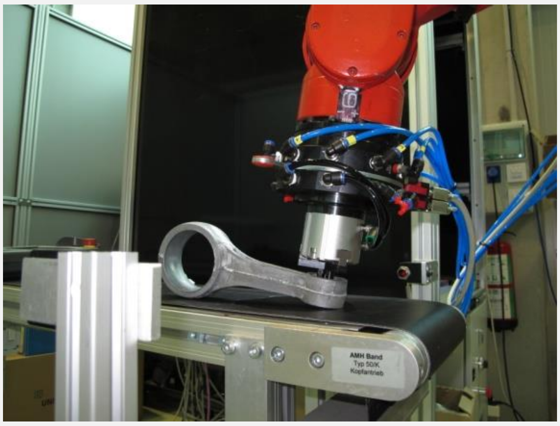

Grasping the rod

2.3 The 2D Station

The elements selected for this station are:

- Camera Genie C1280 1/3” 1280x960 CMOS
- Optics F1.4/16mm
- 24 fps
- 3.75 x 3.75 microns size sensor
- Led lighting

This station is in charge of informing the robot about how to grasp the part. To do it, first a coordinate system has been defined common for robot and for camera. The procedure consists in selecting a common origin for both the robot and camera. This is achieved using a calibrated plate to reference the camera and to use the same calibrated plate without moving it to define the robots local coordinate system, the framework.

Previously the grasping tool has been defined precisely to integrate it into the robot system.

2D station: Camera position

Establishing the common origin

Finally, a further conversion has been performed since the camera Euler transformation, XYZ, was not the same than the transformation used by robot, ZYZ. This is solved first transforming camera pose of the part to the common coordinate system and by performing a second transformation to be equivalent to robot Euler transformation system.

The result of all this calculations is a direct command to the robot to grasp the part.

Grasping pose for rod

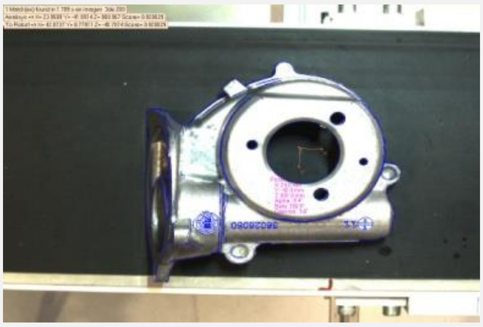

Grasping pose for part 1

2.4 The 3D Station

The elements used in this station are:

- Two Camera Genie HM1400 monochrome 1400x1280 CMOS
- Optics F1.4/16mm
- 64 fps
- 7.4 x 7.4 microns size sensor
- Laser line generator: Z-Laser Z030M18H-F450LP30 (blue, 30mw, 450 nm and with a LP30 optic)
- Band pass filters: IBP470 centered at 470 nm

On the final integration of the 3D system workstation, the image acquisition will be done by firing capture of only one trigger pulse: the start. The acquisition consists of a fixed number of frames obtained over the lineal movement of the robot at constant speed. This procedure may look less precise than an encoder triggered acquisition, but it is considered due to the fact that the part will be moved, under the cameras, by the robot. An encoder acquisition approach on the robot requires to convert, in a parallel task, actual positions into pulses, checking actual position against a desired increment of displacement. The exact determination of the increment may be imprecise or slow. Instead, the frame rate is considered constant frequency in the camera acquisition system since no analysis will be included during the robot movement. The movement of the robot can be precisely considered as totally linear. A procedure to coordinate images frame rates with robot speed to correlate movement with real dimensions will be needed.

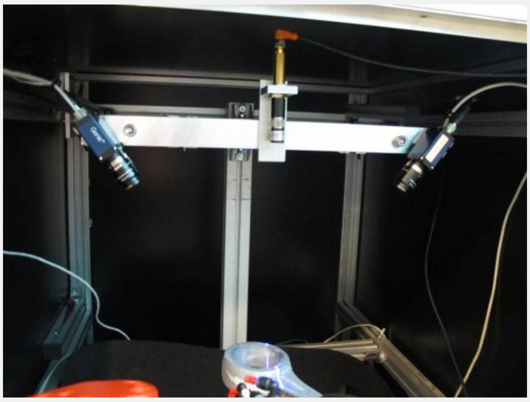

Rod under 3D cameras

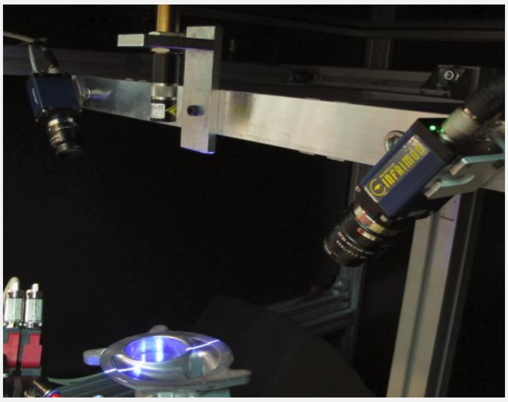

Part 1 on 3D station

2.4.1 3D reconstruction and partial view registration

The sheet of light setup used for 3D reconstruction is a dual camera system, in a reversed ordinary setup configuration. The reversed ordinary setup provides a good height resolution avoiding miss-register problems. The height resolution obtained with this setup can be expressed as follows:

$$\Delta z \approx \frac{\Delta x}{\sin(\alpha)} \tag{1}$$

The dual camera system is mounted in the direction of the relative movement of the part under inspection, so occlusions due to geometry are avoided. This setup can be seen in the next figure. Additionally, for each camera, calibration has been performed so that the partial point clouds are obtained directly in real world coordinates, in this case, mm, which are the units in the part STL model.

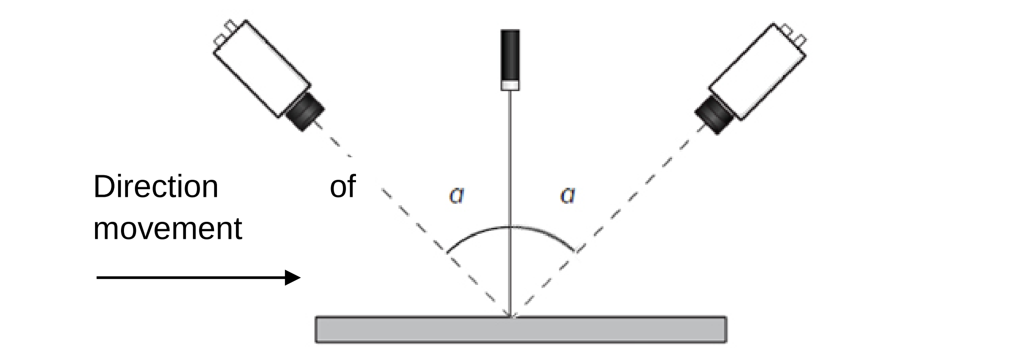

Schematics of the dual camera laser triangulation system, in reversed ordinary setup.

To optimize the acquisition of both cameras a trick was used that served to improve the cameras acquisition rate from 64 fps to 120 fps.

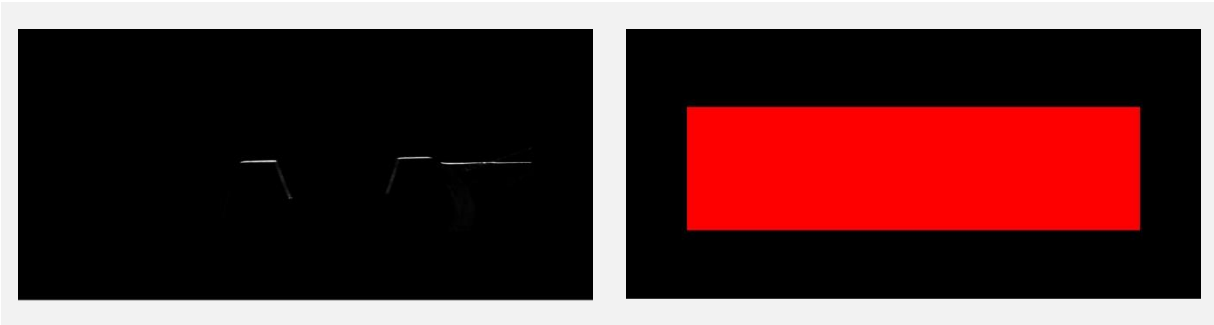

Profile ROI

To improve the acquisition rate, the dimensions of the acquired images are configured to have the size of the ROI (Region Of Interest) that comprises the laser profile. This allowed us to acquire at a faster pace. To use the calibration of the camera that is based on the entire image, we filled the rest of the image in black. We did not need a real capture of the entire image but only the acquisition of a frame that has the size of the ROI. After acquisition and before analysis, a complete image is reconstructed to be able to use the calibration of the camera on its full size. This reconstruction is done after the real acquisition of the camera prior to its analysis, that will be done while the robot is moving away from this station.

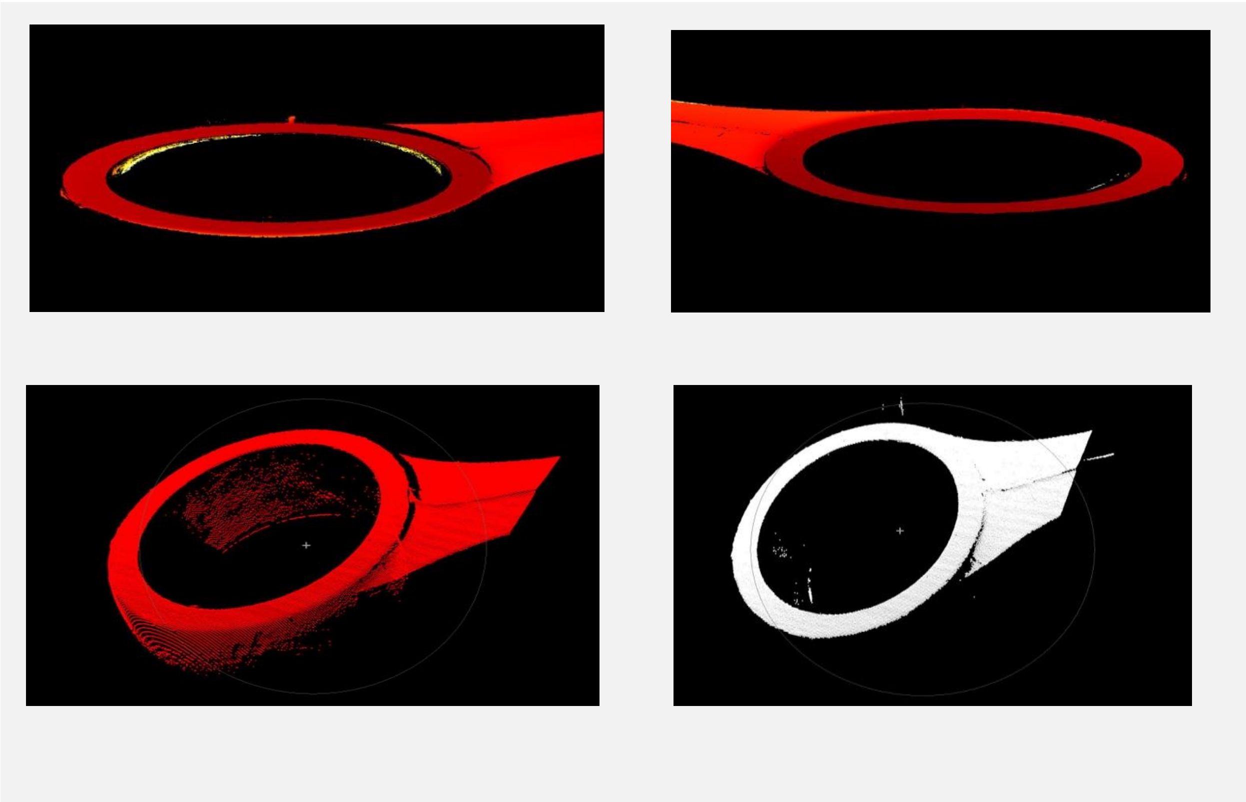

3D Representation of result from camera 1   3D Representation of result from camera 2

For the registration of both partial reconstructions obtained from the part, key points have been extracted using the scale-invariant feature transform algorithm. Having obtained the key points, the registration is performed in two steps, first using FANN algorithm for initial registration of clouds, and ICP in a second step to minimize errors, obtaining as a result the affine transformation of the point cloud of the second camera with respect to the other, taking as coordinate reference the first camera in the sense of movement:

$$H_{registration} = H_{icp} H_{fann} = \begin{bmatrix} R_{icp} \cdot R_{fann} & R_{icp} \cdot t_{fann} + t_{icp} \\ 0 \quad 0 \quad 0 & 1 \end{bmatrix} \qquad (2)$$

Transforming the second partial point cloud by Eq. 2 and adding the points to the first point cloud taken as reference, a first registration step is achieved. This initial step can be seen in the next figure:

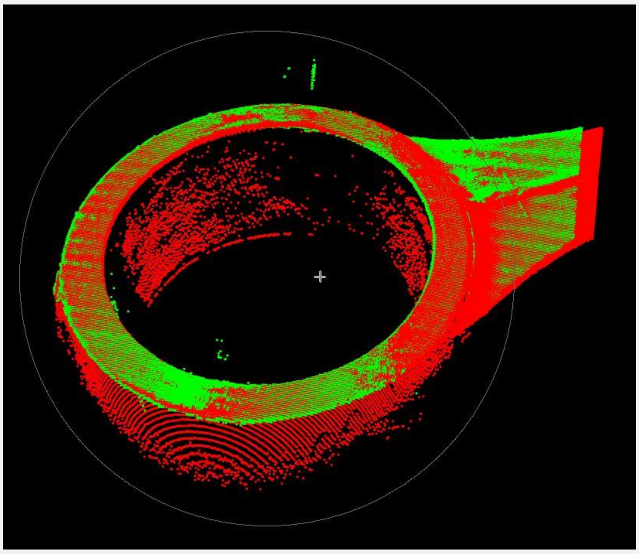

Registration of the two partial point clouds (red and green) obtained.

2.4.2 Point cloud preprocessing

After obtaining the registered point cloud, further processing is needed to obtain a suitable 3D volume to be compared against the STL model of the ideal part. All needed configuration parameters in the different operations have been fixed empirically after performing some tests, and taking into account the characteristics of the initial point clouds in terms of number of points and spatial resolution in X and Y axis. The operations applied on the point cloud are listed and briefly described below in order of application:

- Outlier removal: Using the euclidean distance as measuring criterium, an outlier in the point cloud is defined as a point whose mean distance to the k nearest neighbours is bigger than D mm, with k = 3 and D=5.
- Downsampling using a voxel grid filter: All the points within voxel cubes of edge d millimeters, are substituted by a new point, the cube centroid. Voxel cubes containing less than n points are removed from the point cloud. d = 0.5 mm, n = 5 points.
- Smoothing of the downsampled point cloud. For point cloud smoothing MLS algorithm is used. MLS smoothing algorithm fits a planar surface or a higher order polynomial surface to its k nearest points. The surface fitting is a standard weighted least squares parameter estimation of the plane or polynomial surface parameters, respectively. The closest neighbours of P have higher contribution than the other points, which is controlled by the following weighting function with a parameter φ:

$$w\left(P^*\right)=e^{\left(-\frac{\left\|P^*-P\right\|^2}{\varphi^2}\right)} \tag{3}$$

The point being processed is then projected to the calculated local surface, with a relative φ = 1.0.

Applying these three steps to the initial registration process, a smoothed model with less noise is obtained, suitable to be used for detecting burrs in the part, when comparing it with the CAD model of the part or when comparing it with a part of production, “first model” used as a reference. Next figure shows the final model of the part reconstructed.

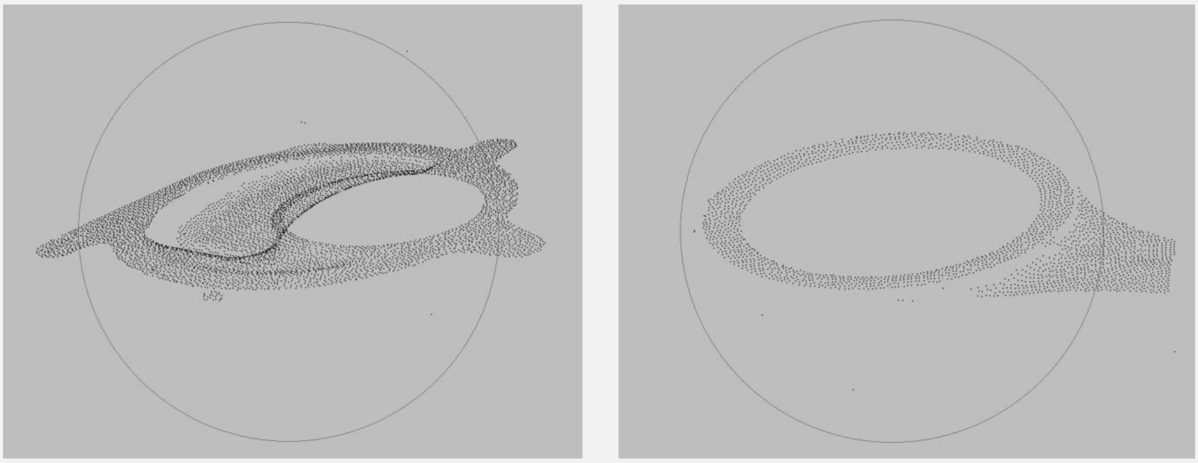

Final model after outlier removal, downsampling and smoothing.

2.4.3 Matching with a reference model for burr detection

For burr detection, the registration and posterior generation of the point cloud model of a new part, generated as documented in the previous section, is used to compare it against a first cloud model of a reference part. The registration operation is based essentially in the same procedure explained, taking as point clouds to register the generated 3D model from the scanned part by each camera. Once the complete registration is performed, distance from the scanned part to nearest model surface is calculated, by establishing a threshold in distance, points whose distance is over that threshold are marked as burr points.

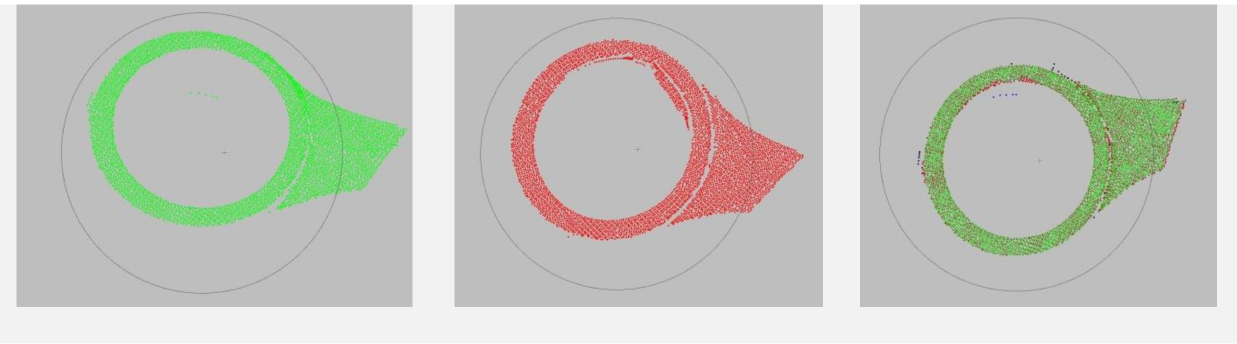

Reference Tested Result

The last step is a 3D clustering of these points, to obtain position and size of the burrs to be removed by the laser. The result obtained in a graphical basis is then transformed numerically to get the coordinates of the burrs.

On the next figures the (x,y,z) representation of both parts is shown. Inside each part, the representation of the reference part is in blue while the tested part is highlighted in red.

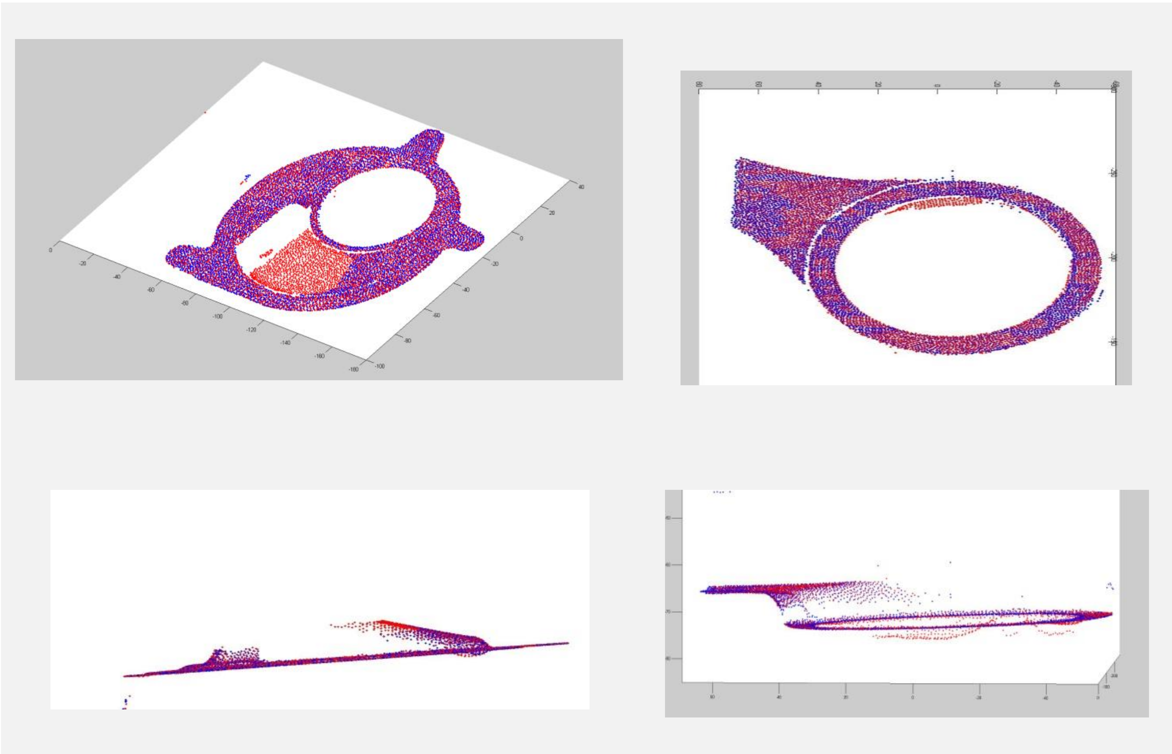

Burrs part 1 Burrs part 2

A more detailed view shows the bur presence on the analysed part.

This procedure, to check against a reference part, has been selected to include those situations where there is a lack of a valid CAD of the part or in those cases where it may present, for whatever reasons, slight changes with the produced part. For a generic solution, we chose to compare the part with a reference, obtained from the same batch.

3 The debur process

This section deals with the test runs on real parts, mainly connecting rods, using all the steps proposed by DEBUR approach, and also with the design and implementation of monitoring methods for pierce and quality evaluation during the final laser deburring/cutting process, which once further developed and fine-tuned, could be used as the basis for a control loop.

3.1 Deburring tests on real parts

One of the goals of this task is to make a first test of the complete system on real parts. In order to do so, first a geometry has been selected, chosen form the preselected pool of possibilities. In this case, due to its simple geometry, decent sized burrs and relatively easy access to their location, the connecting rod has been chosen in order to have a first evaluation of the cell perfomance. In this particular rod design burrs appear mainly around the perimeter at the locations shown in the following picture.

General view of the connecting rod and detail of burr location

The burrs might appear anywhere around the perimeter in the inner face of the top side (that with the hole of highest diameter) of the connecting rod. The thickness measurements carried out by the use of a caliper show that they remain below 0.5 mm, around 350-400 µm.

The process chain, which encompasses all the steps described previously, has been documented and recorded, and the edited video can be freely accesed at the media section in the website of DEBUR project, namely at:

http://deburexperiment.eu/videos/

Regading process parameter details, since the monitoring system is not completely finished, this set of trials has been carried out without any type of monitoring or control system, which means that the tests are in open-loop configuration using constant parameters. Achivable cuts have been found using the parameters which are shown in the following table.

Parameters	Value
Laser power	200 W
Processing speed	25-100 mm/min
Laser tip diameter	2 mm
Type of gas	Ar
Gas pressure	6 bar
Laser spot diameter	~ 30 um
Rayleigh length	0.7 mm

However the results show a somewhat imprecise cutting line, deviating from the ideal trajectory, and a manual correction and redefition of trajectory points by teaching method has been found necessary in this first set of trials. A further fine tunning of this final step is necessary in order to fully complete the automated process chain. Final validation through quality metrics and evaluation of productivity is left for the final task of the project.

3.2 Monitoring of laser deburring process

The cutting process emits radiation with different origins: back scattered radiation from the laser beam, direct penetration of the laser beam, fluorescence of material compounds, plasma radiation and black body radiation. We have focused on the backscattered light. This radiation contains information about the quality of the process that could serve for process controlling tasks. In fact, when the material is not well cut, the laser beam does not completely penetrate the material sheet and high levels of backscattered radiation are produced. Discrimination between normal and high levels of backscattered radiation is the key for the monitoring and controlling tasks.

In order to capture the backscattered radiation of the laser beam, a photodiode has been used. The main challenge for this kind of sensor is to capture light symmetrically. For this, a bundle of optic fibers 1:4 have been selected. One side of the bundle has 4 fiber optics that have been placed symmetrically around the laser head nozzle by using a custom made adapter. The remaining side of the bundle is attached to a photodiode with a transimpedance amplifier. In the following figure, a diagram of the photodiode and fiber bundle is shown. Next figure shows a picture of the current assembly attached to the laser head.

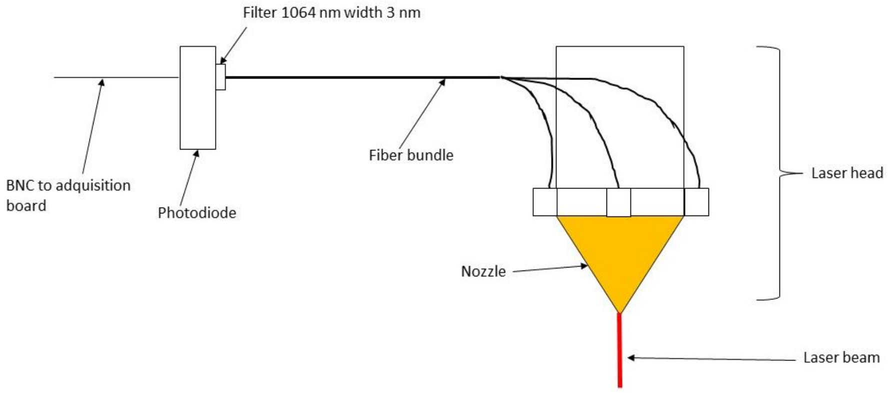

Diagram of the photodiode and fiber bundle

Laser head with adapter and optical fibers (in orange)

In the following figure, it is shown the photodiode signal captured during the cutting process of a small rectangle in stainless-steel (thickness 1 mm) using different parameters. As the signal captured by the photodiode is a portion of the scattered laser light, one should expect low signal during an optimum cutting process. This is because in a cutting process the laser beam penetrates the material forming the well-known cutting front of melted material in the direction of the laser head movement. High levels of scattered laser light would mean that the material is not effectively cut and therefore either cutting speed or laser power are not suitable for the material and cutting trajectory. In this figure, the process parameters have been adjusted in order to obtain an optimal result. The photodiode signal shows that the overall measured level decreased by optimizing the cutting parameters.

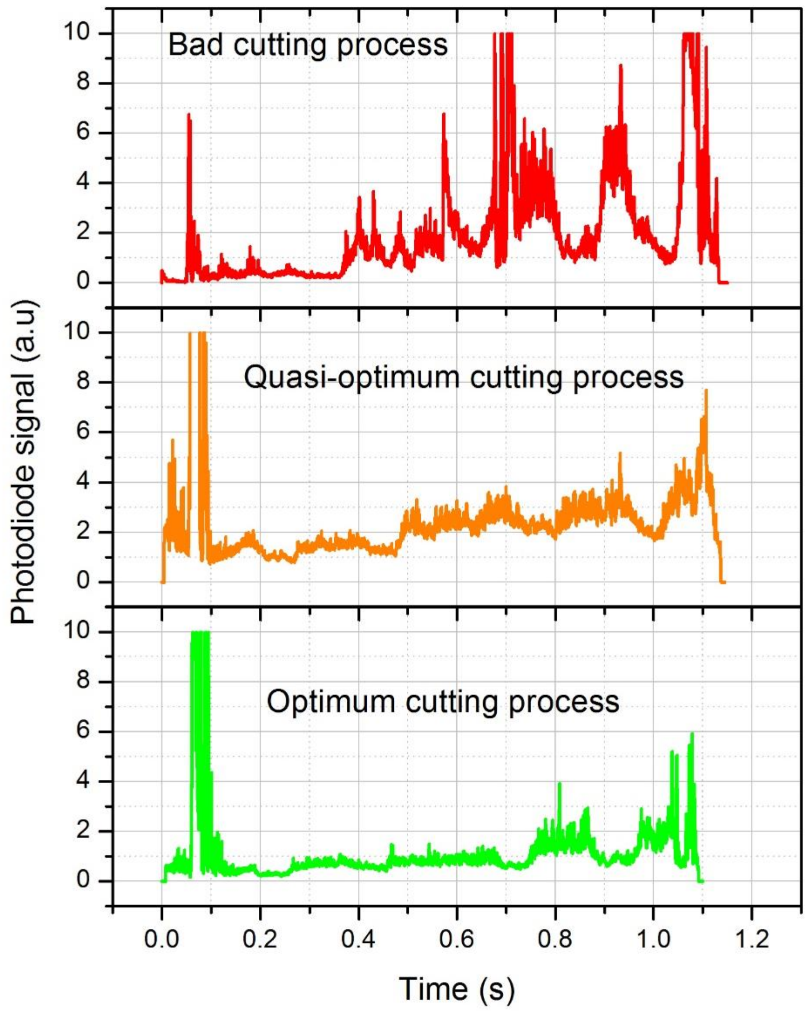

Photodiode signal captured during the cutting process of a small rectangle in a sheet of stainless-steel (thickness 1 mm)

At times between 0.05 and 0.1 s we however record high levels of the photodiode signal in the three cases. This has to do with the also well-known piercing effect. In fact before forming the cutting front, the laser beam has to penetrate all the thickness of the material. During this, most of the laser light is absorbed by the material, but there is also a significant portion of the light that is back scattered. This gives rise to an enhancement of the photodiode signal. Once the laser penetrates the material, the signal decreases and a cutting front is formed. Low levels of the scattered light are then emitted by the interaction area.

4 Cell integration

This section is divided in two parts, the cell integration of the different elements and the HMI developed for cell information on operation.

4.1 Central unit: the robot

The coordination of the different systems of the cell is done by the robot CPU. The robot is assisted by a PC that is in charge of vision analysis and burr calculations on the manipulated part.

The robot is in charge of the cell automation, that is, the conveyor and the laser power control. As it moves through the different workstations, it triggers the different analysis that are solved by the analysis PC.

Two communication layers have been developed and are centralized by the robot:

- one digital I/O with the conveyor and with the laser control and
- an Ethernet layer with the analysis PC.

The third control level is a result of the analysis done on the PC. This result is passed to the robot to optimize the process pointing the path areas where speed can be optimized and the parts of the path were burrs were found.

4.1.1 Cell Automation layer

This level solves all the automatism of the cell:

- Conveyor control
- Lighting the part on the 2nd workstation
- Laser control

This first layer is responsible for low level digital communications. It is based on the digital I/O of the robot. This layer is governed by the robot and controls the movement of the conveyor, the lighting for the 2D cameras and the activation of the laser beam.

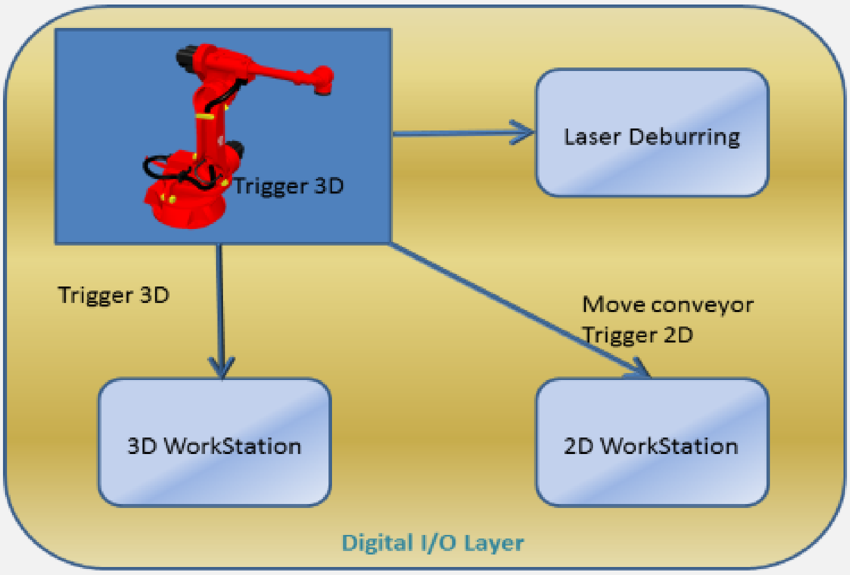

The I/O communications layer

4.1.2 Ethernet layer

The second layer is a high level communication layer that uses TCP/IP Ethernet protocol for communication. A portable PC with high specifications: graph capacity and fast processing characteristics to handle the two 3D cameras, the point cloud analysis is at the same time in charge of the control of the cell.

Over this layer, the laptop communicates to the robot, the pose of the part to be grasped and analyses the 3D real model of the part. It also extracts the burr locations and sends the robot the trajectory corrections based on their position and size.

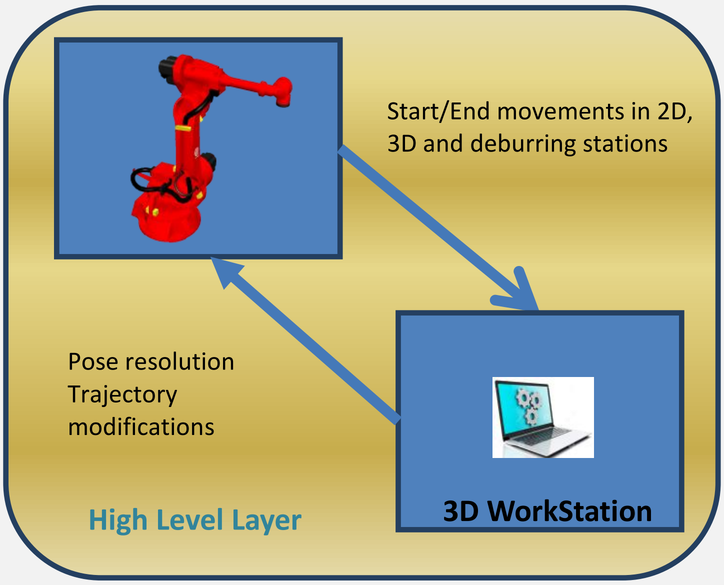

The ethernet communication layer

4.1.3 Robot path optimization

Generally, in aluminium casting alloys, the areas where burrs are to be treated usually appear along the closure line of the mould. On the Deliverable D 2.1 there were some images showing where the burrs may appear at part type 1.

Burs on part 1

Burs area on rod

On the CAD, the areas of the part where burrs may appear are defined. The deburring trajectory of the robot is defined using the CAD.

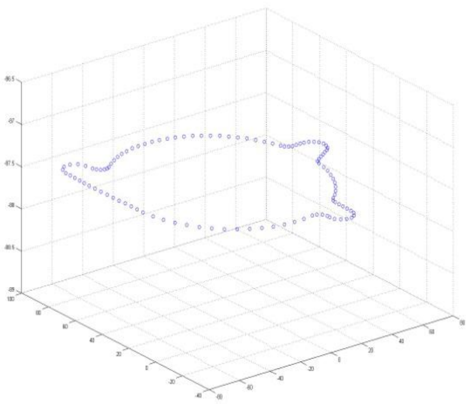

Robot path from CAD: burrs area

	x	y	z	descriptor
Point 1	-100.33	-24.76	40.65	d1
Point 2	-100.72	-24.33	42.85	d2
Point 3	-101.07	-23.21	44.80	d3
Point 4	-101.33	-21.51	46.30	d4
Point 5	-101.48	-19.41	47.17	d5
Point 6	-101.51	-17.14	47.34	d6
Point 7	-101.41	-14.94	46.78	d7
Point 8	-101.20	-13.03	45.55	d8
Point 9	-100.89	-11.63	43.78	d9
Point 10	-100.51	-10.87	41.67	d10
Point 11	-97.19	-25.42	22.80	d11
Point 12	-97.54	-25.35	24.78	d12
Point 13	-97.89	-25.27	26.77	d13
Point 14	-98.23	-25.20	28.75	d14
Point 15	-98.58	-25.13	30.73	d15
Point 16	-98.93	-25.05	32.72	d16
Point 17	-99.28	-24.98	34.70	d17
Point 18	-99.63	-24.91	36.68	d18
Point 19	-99.98	-24.84	38.67	d19
Point 20	-100.33	-24.76	40.65	d20
Point 21	-90.36	-24.39	-15.93	d21
Point 22	-91.11	-24.50	-11.63	d22
Point 23	-91.87	-24.62	-7.33	d23
Point 24	-92.63	-24.73	-3.02	d24

Robot path points definition plus descriptor

On the 3D station the 3D point clouds obtained will be used to measure the burrs in these specific regions. The analysis will give as result the size and position of burrs. The robot trajectory generated by the CAD will be completed with descriptors accessible from the central unit of the cell. Then, the information coming as result of the 3D analysis of burrs will modify robot behaviour, in the form of start/stop instructions and trajectory optimization through these externally modified values.

Every CAD point is transformed to a robot instruction in the form:

MoveL Offs(p_initial, ***δ*x, *δ*y, *δ*z**), **v_d1**, z5, t_debur \WObj:=wobj_laser;

Every robot movement is commanded defining the offset from the initial point δx, δy, δz. The 3D station defines the command speed to be applied v_d1 that is determined on the 3D measurement workstation.

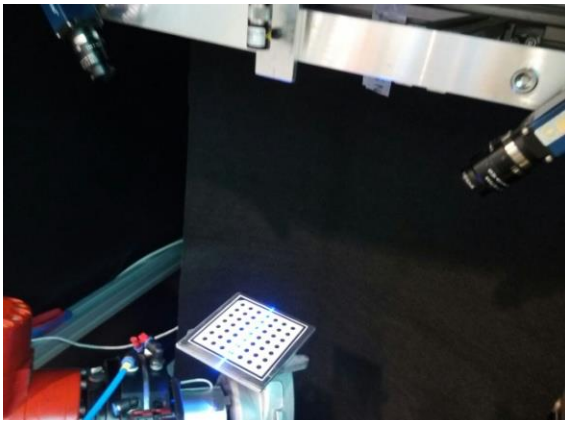

Setting origin to the correct grasping variations

This way, the result of the 3D analysis will be parameterized and integrated in the robot trajectory. The value of this parameter/descriptor will serve to control the speed of the TCP of the tool. When this parameter is high due to the detection of high size burrs, it will command lower speed and when this parameter is low due to the absence or detection of small size burrs, it will serve to command higher speed.

The generation of the robot trajectory will be done automatically at the 3D workstation, rewriting the CAD points to robot movement instructions.

4.2 HMI

The HMI that controls the analyses done on the cell is network connected to the robot, therefore endowing it with analysis functionalities.

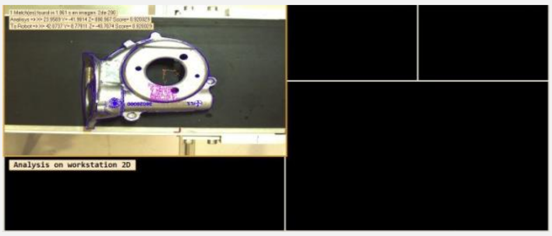

2D area, below messages are for operator

3D area, below left operator area.

In the PC that is in charge of the analysis, the connection to the robot is established in the first place, and from that moment on, it is ready to make the different analysis needed by the robot to correctly control the cell.

- 2D processing
- 3D analysis
- Path adjustment.

The operator of the cell is then able to see the results on the monitor of the laptop.

Three main areas conform the communication with the operator:

- 2D analysis and results
- 3D analysis and results
- Messages to operator.

This HMI design and working procedure has been developed and prepared mostly using Halcon and Matlab. The final result is then compiled to VisualC. This procedure will be validated on the following task.

5 Conclusions

- The deburring cell has been designed and constructed and is ready to operate with the two selected parts. This comprises:
    - The conveyor belt module is operative.
    - The 2D station is operative.
    - The 3D station is operative.
    - The robot with a manual tool change for laser operations, grasping and 3D analysis tuning is also operative.
    - On-line monitoring deburring process is ready and it is being tested on real parts.
    - The HMI is already done.
- The deburring cell is now ready for validation.